Interface Synergistic Effect of NiFe-LDH @ 3D GA Composites towards Efficient Electrocatalytic Water Oxidation

Xiaohui Guo *, Jiangcheng Zhang , Qiuhan Cao , Xin Yu , Hu Yao , Baolian Su

Posted Date: 1 October 2024

doi: 10.20944/preprints202409.2438.v1

Keywords: NiFe-LDH; graphene aerogel; synergistic effect; OER; activity

 doi:10.20944/preprints202409.2438.v1

Article

Interface Synergistic Effect of NiFe-LDH @ 3D GA Composites towards Efficient Electrocatalytic Water Oxidation

Jiangcheng Zhang [1], Qiuhan Cao [1], Xin Yu [1], Hu Yao [1], Baolian Su [2] and Xiaohui Guo [1,*]

[1] Key Lab of Synthetic and Natural Functional Molecule Chemistry of Ministry of Education, The College of Chemistry and Materials Science, Northwest University, Xi'an 710069, P. R. China
[2] Department of inorganic chemistry, University of Namur, 61 rue de Bruxelles, B-5000 Namur, Belgium
* Correspondence: guoxh2009@nwu.edu.cn

Abstract: Currently, NiFe-LDH exhibits excellent oxygen evolution reaction (OER) due to the interaction of the two metal elements on the LDH platform. However, such interaction is still insufficient to compensate for its poor electrical conductivity, limited active sites and sluggish dynamics. Herein, a feasible two-step hydrothermal strategy is proposed by coupling low-conductivity NiFe-LDH with 3D porous graphene aerogel (GA). Consequently, the optimized NiFe-LDH/GA (1:1) possess a 257 mV (10 mA cm^{-2}) overpotential and could continuously operate for 56 h in OER. Our investigation validates that the NiFe-LDH/GA has a three-dimensional mesoporous structure, synergistic interaction between LDH and GA, and interfacial reconstruction of NiOOH. Such interface synergistic coupling effect promotes fast mass transfer and facilitates OER kinetics, and this work offers new sights into designing efficient and stable GA-based electrocatalysts.

Keywords: NiFe-LDH; graphene aerogel; synergistic effect; OER; activity

1. Introduction

The search for sustainable energy sources and technologies to solve the energy and ecological problems stemming from the consumption of limited fossil fuels has emerged as a critical priority [1]. It is now well recognized that OER plays a pivotal role in numerous sustainable energy technologies, such as the electrochemical decomposition of water [2], carbon dioxide reduction reactions [3,4]. However, the OER process involves multiple steps of four electron transfer and the generation of O_2, resulting in its slow reaction kinetics. OER requires extremely high overpotentials, resulting in its not yet meeting the practical requirements for energy conversion and storage [5]. Consequently, it is vital and urgent to explore advanced OER catalysts with high catalytic activity and high stability.

Transition metals (TMs) have the advantages of being abundant, environmentally friendly and inexpensive, so researchers have made a lot of studies on effective electrocatalysts of TMs, including alloys [6], LDHs [7], transition metal oxides [8] phosphides [9], nitrides [10], and sulfur group compounds [11]. Specially, LDHs have been widely used in the fields of electrolysis and electrolytic catalysis, which is attributed to their affordability, high theoretical activity, diverse composition, and simple preparation [12–14]. However, LDHs have insufficient electrical conductivity and are prone to problems such as build-up and aggregation [15,16]. This seriously affects the exposure of the more active center of the catalyst and the electron transfer process, thus greatly affecting its catalytic activity and stability [17,18].

Various schemes have been proposed to improve their conductivity and stability, with a very feasible approach being the integration of LDHs with conductive carbon substances, like CNTs, GO[19,20], MXenes and Nitrogen doped carbon [21,22]. The resulting catalysts can improve the drawbacks of LDHs, thereby substantially enhancing the OER performance. For example, Wang et

 doi:10.20944/preprints202409.2438.v1

al. Reported that Nanodots of NiFe-LDH with a high concentration (47 wt%) were cultivated on N-doped 3D porous carbon substances. NiFe-LDH/3D MPC's distinctive architecture addresses NiFe-LDH's issues with less conductivity and exposure to active sites, leading to outstanding ORR and OER characteristics [23]. Rinawati et al, synthesized novel doped heterogeneous atoms GQDs and doped them into MOF-derived NiFe-LDH. The catalyst exhibits very high catalytic activity in alkaline media [24]. Although LDHs composites have made good progress in electrocatalytic hydrogen and oxygen production, the two-dimensional conductive substrate is not a good solution to the problems of easy aggregation of LDHs and slow mass transfer rate. Therefore, it is necessary to construct LDHs composites with 3D conductivity substrate. GA has the benefits of large porosity, superior electrical conductivity, resistance to corrosion, extensive specific surface area, fast mass/charge transport, and stable electrocatalytic performance, which is considered as a very ideal conductive substrate [25–27].

Based on the above considerations, a composite catalyst combining NiFe-LDHs with 3D porous GA was prepared through simple hydrothermal reaction and the following freeze-drying process. The unique 3D porous structure, large specific surface area and the interfacial synergistic coupling effect between GA and metal active sites jointly improve the charge transfer process and reaction kinetics of OER. The results show that NiFe-LDH/GA (1:1) exhibits a low overpotential of ~ 257 mV (10 mA cm^{-2}), the Tafel slope is down to 49 mV dec^{-1}, and displays excellent electrochemical stability for over 56 h continuous electrocatalysis in OER. In conclusion, this endeavour provides a viable approach for the development of cost-effective aerogel composites for potential catalysis, energy storage and energy applications.

2. Experimental Section

2.1. Synthesis of NiFe-LDH

In a typical synthesis of NiFe-LDH(2:1), 1.34 mmol of $Ni(NO_3)_2{\cdot}6H_2O$, 0.66 mmol of $Fe(NO_3)_3{\cdot}9H_2O$, and 1 mmol of urea were dissolved in a mixed solution of deionized water (DIW, 2 ml) and ethylene glycol (EG, 8 ml). The blend was moved to a Teflon-lined steel autoclave following 30 min of agitation. Then the autoclave was heated at 180 ℃ for 12 h. After cooling down, the sample was washed several times, then dried by freeze dryer. The synthesis process of NiFe-LDH(3:1), NiFe-LDH(1:1), NiFe-LDH(1:2) and NiFe-LDH(1:3) is the same as NiFe-LDH(2:1), with the only difference is the molar ratio of nickel and iron metal salts, respectively.

2.2. Synthesis of 3D NiFe-LDH/GA

3D NiFe-LDH/GA was prepared by adding different qualities of NiFe LDH to 10 ml of GO solution (2 $mg{\cdot}ml^{-1}$) and sonicate for 3 h. Then the mixture was transferred to a Teflon-lined steel autoclave and heated at 180 ℃ for 6 h. After cooling, the samples were performed freeze-drying. The obtained material was named as NiFe-LDH/GA. Different catalysts were synthesized as the same method except adjusting the mass ratio of NiFe-LDH to GO 2:1, 1:1 and 1:2.

2.3. Characterization

The X-ray diffractometer (Bruker D8 ADVANCE*) was used to characterize the crystal structures of the different NiFe-LDH/GA. The scanning electron microscopy (SEM, SU-8010) and the field-emission transmission electron microscope (FEI, Talos-200, USA) were used to characterize the morphology of the samples. The element components and chemical states of samples were measured by X-ray photoelectron spectroscopy (XPS, PHI5000 VersaprobeIII XPS). The element distribution of NiFe-LDH/GA was determined by EDS mapping at an accelerating voltage of 200 kV.

2.4. Electrochemical Measurements

All electrochemical tests of the OER were recorded with an electrochemical work station (CHI660E) using a three-electrode system, with Hg/HgO (1 M KOH) used as the reference electrodes, while Pt foil and CP loaded with catalyst (1*0.5 cm^{-2}) was employed as counter and working electrodes, respectively. The working electrode was prepared by the following method: 5mg of

 doi:10.20944/preprints202409.2438.v1

sample, 50ul of Nafion (5 wt.%) and 950ul of ethanol solution were mixed by sonication. Then, 30 μL of the inks obtained in the previous step was added to CP (1 x 0.5 cm^{-2}), and natural drying. The materials loads on the CP was about 0.3 mg cm^{-2}. Commercial catalyst (RuO_2) as a comparison. Performance of the OER was evaluated using cyclic voltammetry (CV) and linear sweep voltammetry (LSV) (with scanning speeds of 50 mV s^{-1} and 5 mV s^{-1}, respectively). Electrochemical impedance spectroscopy (EIS) was performed in 1 M KOH solution over a frequency range of 0.01 Hz - 100 kHz, with an amplitude of 5 mV. Electrochemical double-layer capacitances (C_{dl}) were measured via cyclic voltammograms from 1.124-1.224 V *vs*. RHE, where Faradic current is absent. C_{dl}'s value was determined by plotting half the variance between anodic and cathodic current densities in relation to the scanning rate. The catalyst was subjected to long-term cycling testing at a constant current density (10 mA cm^{-2}). All the measured potentials were standardized to the reversible hydrogen electrode (RHE) using the equation: $E_{RHE} = 0.0977\ V + 0.059 \times pH + E_{Hg/HgO}$.

3. Results and Discussion

At first, the 3D NiFe-LDH/GA catalyst was prepared by two-stage hydrothermal reaction and the freeze-drying processes, as depicted in Figure 1a. The physical phase composition and crystal structure of NiFe-LDH/GA and NiFe-LDH was characterized by X-ray diffraction (XRD) technique (Figure 1b). For NiFe-LDH, the peaks at 9.75°, 18.04°, 33.75°, 36.76°and 60.1°are indexed to (003), (006), (012), (015) and (110) facets of NiFe-LDH, respectively [28], indicating successful synthesis of NiFe-LDH/GA. However, the peak intensity is faint, indicating the low-crystalline nature. In addition, as the amount of Fe element increases, there only displays the characteristic peak of FeOOH (Figure S1). When NiFe-LDH was integrated with GA, the NiFe-LDH/GA still has the characteristic peaks of NiFe-LDH material, indicating that GA does not change the lamellar structure. It is worth noting that the peak strength of the material became higher, indicating that the addition of graphene oxides in the secondary hydrothermal process enhance the crystallinity of NiFe-LDH, which prove the strong interaction of the two components. Compared with NiFe-LDH/GA (1:1) and NiFe-LDH/GA (2:1), the characteristic peaks of NiFe-LDH/GA (1:2) are weaker, which may be due to less NiFe-LDH added (Figure S2).

In the Raman spectra (Figure 1c), the intensity ratios (I_D/I_G) of the D and G bands of NiFe-LDH/GA (1:1) and GA are 1.03 and 0.85, respectively. This suggests that the integration of NiFe-LDH with GA lead to an increase in the defects on the GA surface. From Figure 1d, the adsorption isotherm of NiFe-LDH/GA (1:1) is similar to the characteristics of type IV adsorption isotherm, and present an obvious h3-type hysteresis line, which suggests that the material has a mesoporous structure [29]. The specific surface area of NiFe-LDH/GA (1:1) is measured to be 122.59 $m^2\ g^{-1}$, which is significantly higher than that of the previously documented LDH/GA composites [30,31]. Meanwhile, Figure 1e indicates that the average pore diameter of the composites is around 2.85 nm, further confirming the mesoporous structure of NiFe-LDH/GA (1:1). The larger specific surface area provides more active sites, and mesoporous structure was conductive to reactant transportation and immediate desorption of gases, which in turn improves the catalytic activity.

 doi:10.20944/preprints202409.2438.v1

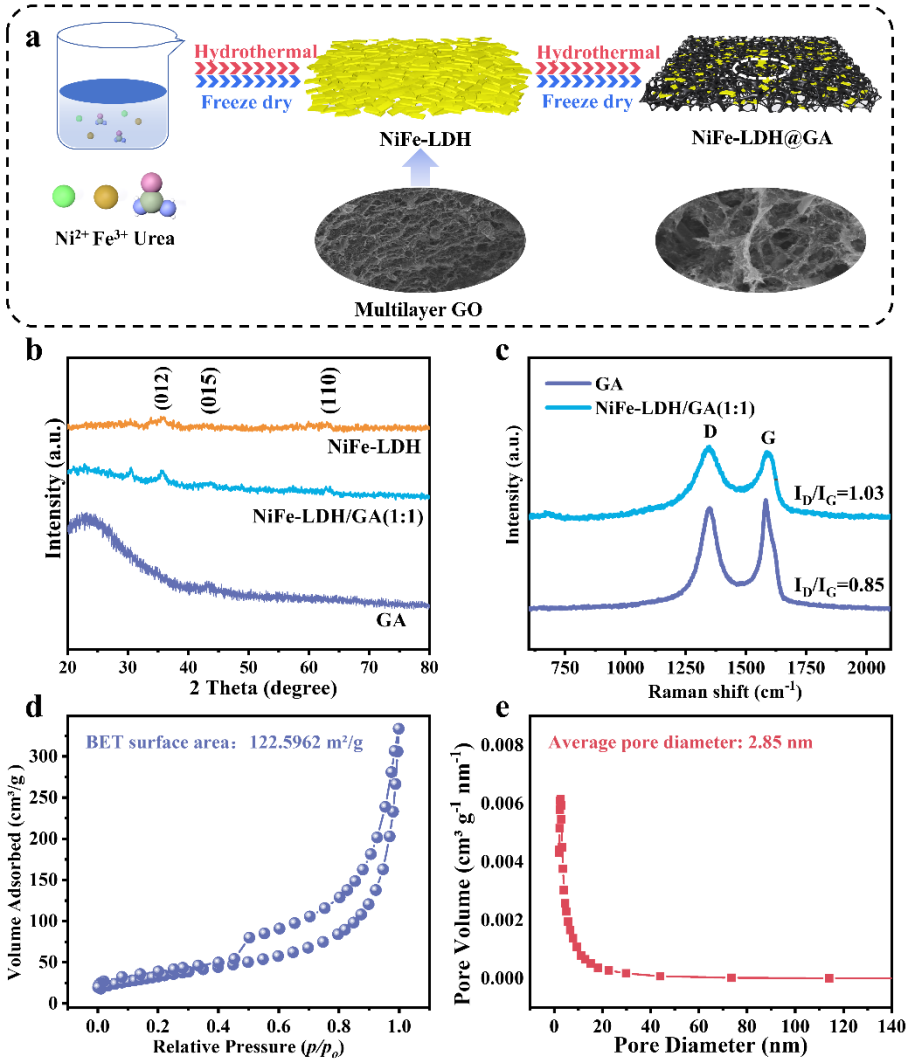

Figure 1. (a) Schematic diagram of the synthesis procedure of NiFe-LDH/GA. (b) XRD patterns. (c) Raman spectra. (d) N_2 adsorption-desorption isotherms and (e) Pore size distributions of the NiFe-LDH/GA (1:1).

The elemental composition and valence states of the catalysts were subsequently characterized using XPS. The overall spectrum of NiFe-LDH/GA(1:1) and NiFe-LDH (Figure S3) manifested the coexistence of Ni, Fe and O. Figure 2a shows the Ni 2p spectra of NiFe-LDH, where it can be seen that Ni^{2+} $2p_{3/2}$ and $2p_{1/2}$ located at 855.12 and 872.88 eV and accompanied by two satellite peaks located at 860.78 and 878.78 eV, respectively [32]. The Fe 2p spectrum of NiFe-LDH in Figure 2b shows Fe^{3+} $2p_{3/2}$ and $2p_{1/2}$ located at 709.85 and 723.11 eV, which are quintessential Fe^{3+} peaks, demonstrating that Fe exists in the form of Fe^{3+} in NiFe-LDH/GA(1:1), and there is also a satellite peak (noted as Sat.) located at 713.93 eV [33]. Notably, compared with NiFe-LDH, the Ni and the Fe 2p peak of NiFe-LDH/GA (1:1) were shifted positively by 0.41 and 0.39 eV, respectively, demonstrating that there is a strong electronic interaction and electronic structure change on the interface of NiFe-LDH and GA [32,33]. Figure 2c illustrates the distinct peaks of O 1s of NiFe-LDH/GA (1:1), which can be deconvoluted into three characteristic peaks located at 530.2, 531.2, and 532.63 eV assign to M-O, M-OH, and adsorbed water on the surface, respectively. The C 1s spectra of NiFe-LDH/GA (1:1), the three characteristic peaks at 284.09, 285.34 and 287.81 eV were assigned to the bonds of C-C, C-O, C=O, respectively (Figure 2d). The above results further demonstrate the strong electronic interaction between NiFe-LDH and GA. This strong electronic interaction helps to enhance the catalytic activity and stability of the catalyst [34].

 doi:10.20944/preprints202409.2438.v1

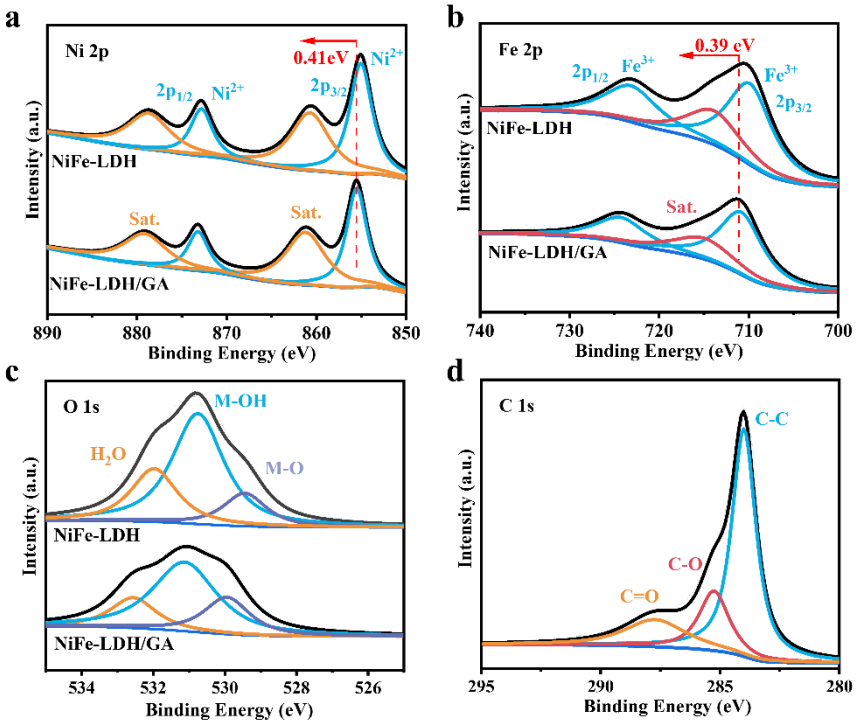

Figure 2. (a) Ni 2p, (b) Fe 2p and (c) O 1s XPS of NiFe-LDH/GA and NiFe-LDH. (c) C 1s XPS of NiFe-LDH/GA.

Figure 3a is a photograph of NiFe-LDH/GA(1:1) composite aerogel. When the whole NiFe-LDH/GA(1:1) composite aerogel was placed on the dandelion, there was no deformation of the dandelion, which indicates that the NiFe-LDH/GA(1:1) composite has an ultra-low density. The NiFe-LDH microstructure is found to be a nanoflower composed of nanosheets (Figure S4). The stacking of these nanoflowers leads to under-exposure of active sites, which in turn reduces the catalytic activity. The original GA is a typical multilayer structure (Figure S5). It was observed from Figure S6 that the microstructure of NiFe-LDH/GA(1:1) is composed of interwoven and entangled rGO nanoflakes, which form a rich 3D pore structure. This unique 3D structure has a large specific surface area conductive to loading of NiFe-LDH and prevent the aggregation of NiFe-LDH, allowing unhindered diffusion and penetration of electrocatalytic active species and thus improving the catalytic activity. From the scanning electron microscope images (Figure S6), it can be seen that the microscopic morphology of the different samples still maintains the three-dimensional network structure. However, when the amount of NiFe-LDH was larger than that of graphene oxide, there was an obvious stacking phenomenon between the graphene flakes, which lead to an obvious reduction of the pores of NiFe-LDH/GA(2:1), which in turn might lead to a decrease in the catalytic activity. Transmission electron microscope (TEM) images (Figure 3b and Figure 3c) show that NiFe-LDH is evenly distributed across the surface of ultra-thin rGO nanosheets full of folds [35]. In the corresponding HRTEM images, NiFe-LDH (012) lattices with a spacing of 0.247 nm can be observed (Figure 3d) [36], and the corresponding graphite lattices of graphene flakes are also clearly visible. Subsequently, HAADF-STEM and its corresponding EDX elemental mapping (Figure 3e) revealed a homogeneous distribution of O, Ni and Fe elements in FeNi-LDH/GA(1:1).

 doi:10.20944/preprints202409.2438.v1

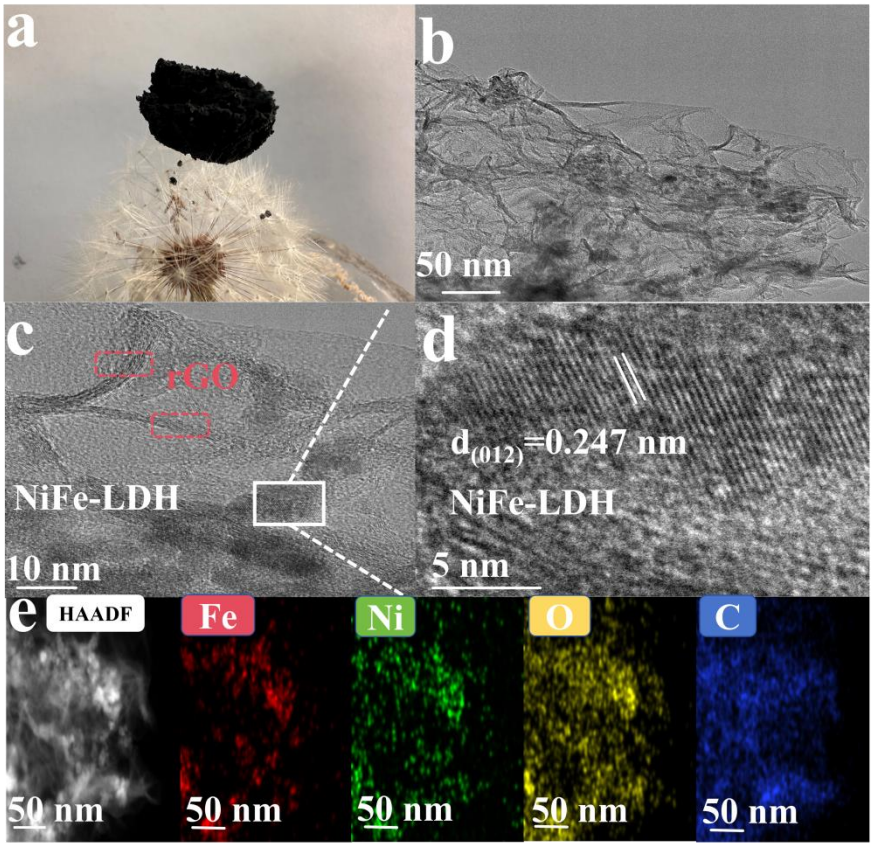

Figure 3. (a) Optical photographs of NiFe-LDH/GA (1:1); (b) TEM image; (c-d) HRTEM images of NiFe-LDH/GA (1:1); (e) EDX elemental mapping images of NiFe-LDH/GA(1:1).

The OER performance of different samples in 1 M KOH solution was evaluated using a three-electrode measurement system. Firstly, the effect of the ratio of metal salts on the catalytic activity of NiFe-LDH was explored (Figure S7). Clearly, NiFe-LDH possess the optimal catalytic activity of OER when Ni:Fe was 2:1. Subsequently, the impact of the mass ratio of NiFe-LDH to GO on the catalytic performance of NiFe-LDH/GA composites was examined (Figure 4a). The overpotential of NiFe-LDH/GA (1:1) was 257 mV at 10 mA cm^{-2}, which is lower than that of NiFe-LDH/GA(2:1) (273 mV), NiFe-LDH/GA(1:2) (287 mV), RuO_2 (310 mV) and NiFe-LDH (287 mV). Typically, the reaction kinetics of a catalyst is evaluated based on the Tafel slope. As illustrated in Figure 4b-4c, the Tafel slope for NiFe-LDH/GA (1:1) was only 46.46 mV dec^{-1}, which was much lower than that for NiFe-LDH(1:2) (87.44 mV dec^{-1}), NiFe-LDH(2:1) (75.74 mV dec^{-1}), NiFe-LDH (88.82 mV dec^{-1}) and 99.6 mV dec^{-1} for RuO_2. As expected, the NiFe-LDH/GA (1:1) has the best electrocatalytic OER kinetics. In comparison, it can be demonstrated that the integration of NiFe-LDH with GA is conducive to acceleratee the kinetics of the OER reaction[37].

Electrochemical impedance spectroscopy (EIS) tests were conducted to deeper into the reaction rates of various catalysts(Figure 4d). The NiFe-LDH/GA(1:1) has the smallest concave semicircle of the Nyquist plot, and its Rct is only 7.341 Ω, which is smaller than that of NiFe-LDH/GA(2:1) (11.02 Ω), NiFe-LDH/GA(1:2) (11.14 Ω), NiFe-LDH (23.52 Ω) and RuO_2 (117.85 Ω) (Table S1). Therefore, NiFe-LDH/GA (1:1) has faster reaction kinetics and charge transfer rate during the OER procedure. It is shown that integrating NiFe-LDH with GA not only effectively accelerates the reaction kinetics, but also enhance of electrical conductivity, which leads to the enhancement of OER activity. Meanwhile, the catalytic activity of NiFe-LDH/GA (1:1) was superior to that most reported LDHs materials and other non-precious metal electrocatalytic catalysts (Table S2). In addition, employing C_{dl} measurements to calculate the ECSA directly, thus further investigate the impact on catalytic performance [38]. The C_{dl} value of NiFe-LDH/GA (1:1) catalyst (13.41 mF·cm^{-2}) was higher than that

 doi:10.20944/preprints202409.2438.v1

of NiFe-LDH catalyst (1.05 mF·cm^{-2}) (Figure S8). The ECSA is directly proportional to the C_{dl}. The larger ECSA imply that catalyst has the more active centers and higher catalytic activity. This indicates that the synergistic interface coupling of NiFe-LDH and GA can result in an increase in the active area, thereby can contribute enhanced catalytic activity in OER.

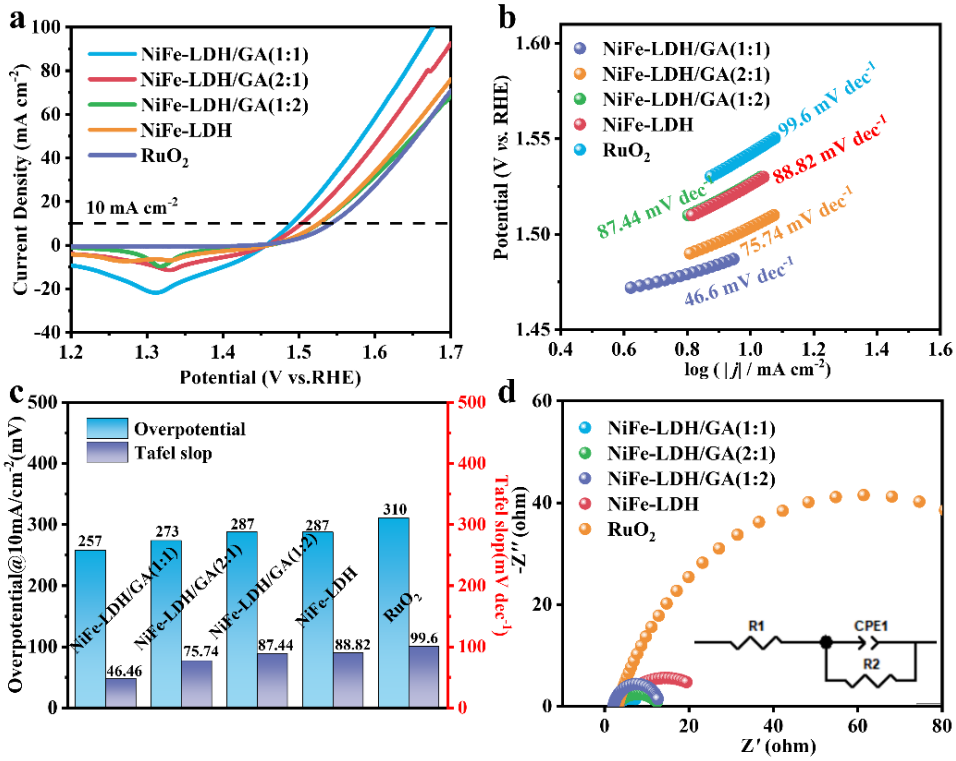

Figure 4. (a) CV curves, (b) Tafel plots analysis, (c) Histogram of Tafel values and overpotentials at 10 mA cm^{-2} and (d) The EIS Nyquist plots of NiFe-LDH, NiFe-LDH/GA(1:1), NiFe-LDH/GA(1:2), NiFe-LDH/GA(2:1) and commercial RuO_2 catalysts.

The durability under alkaline environment is an important consideration when evaluating catalyst performance. Therefore, we performed stability tests on NiFe-LDH/GA (1:1). The CV did not show a notable reduction following 2000 successive cycles (Figure 5a). After 56 h of long-term stability testing, only a 20 mV increase in overpotential was detected, indicating that the catalyst showed excellent durability and efficiency (Figure 5b). The SEM images in Figure S9 showed that the similar layered structure of LDH and the three-dimensional skeleton of graphene are well preserved during operation, which also reveal the effectiveness of the synergistic effect of NiFe-LDH with GA. The post-test XRD analysis showed distinct characteristic NiOOH peaks demonstrating the auto-oxidation process from Ni^{2+} to Ni^{3+} in NiOOH would unavoidably produced on the apparent of NiFe-LDH during OER process (Figure 5c). The Elemental composition and valence of NiFe-LDH/GA (1:1) after the long cycle test were analyzed by XPS. As shown in Figure S10, after 56 h of water oxidation, there were no significant changes in Fe 2p and O 1s. As for the Ni 2p high-resolution XPS, two new peaks appeared at 859.76 and 877.97 eV (Figure 5d), which corresponded to the formation of NiOOH after the OER [39]. This phenomenon also indicates that catalyst reconstruction occurred on the surface of GA during OER, and the newly formed NiOOH directly acts as the real active sites [40,41]. The above test results show that the NiFe-LDH/GA (1:1) catalyst has good catalytic durability.

 doi:10.20944/preprints202409.2438.v1

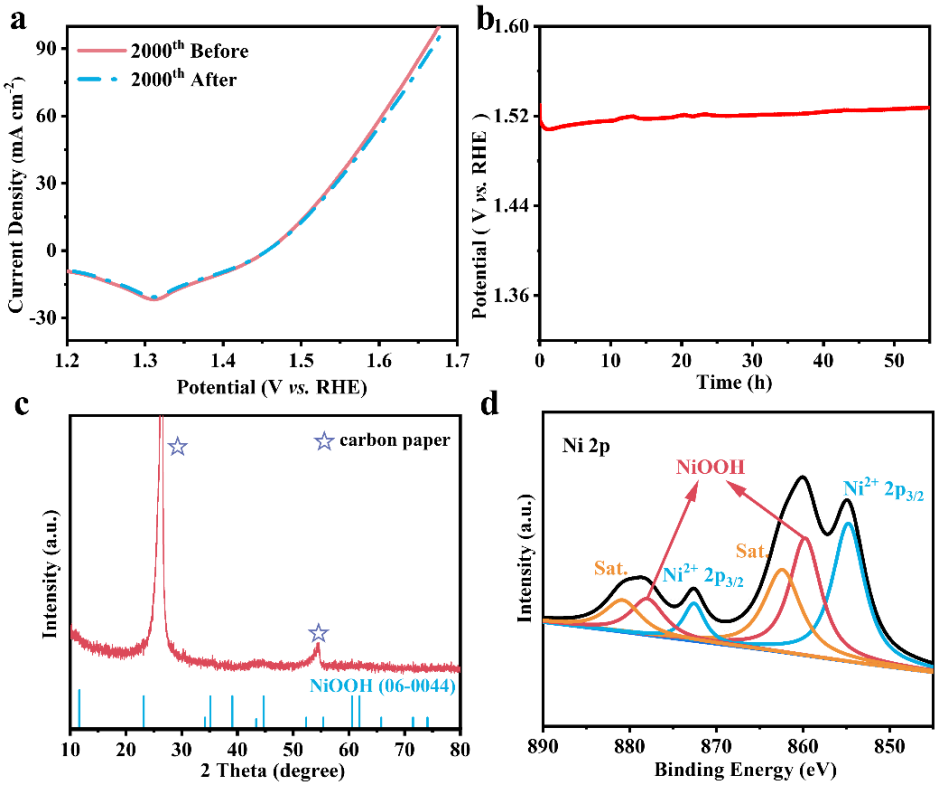

Figure 5. (a) CV curves before and after 2000 CV cycles. (b) Long-term durability tests conducted at 10 mA·cm^{-2}. (c) XRD of NiFe-LDH/GA(1:1) after OER. (d) Ni 2p of NiFe-LDH/GA after OER.

4. Conclusions

In conclusion, an efficient and stable OER electrocatalyst (NiFe-LDH/GA) was successfully prepared. Profited from he excellent electrical conductivity, large specific surface area, numerous active sites and three-dimensional porous channel. The optimized NiFe-LDH/GA (1:1) catalyst possessed a 257 mV (10 mA cm^{-2}) overpotential and good OER stability over 56 h in 1 M KOH, which are superior to most reported NiFe-LDHs and/or commercial RuO_2 catalysts. The synthesis proposed in this work is also applicable to other types of LDHs/GA composites. It offers a new approach for the synthesis of efficient, stable GA-based composites with finely-modulated porous structure and satisfied catalytic performances.

Supplementary Materials: The following supporting information can be downloaded at the website of this paper posted on Preprints.org.

Acknowledgments: This work was supported by the Key projects of intergovernmental international cooperation in the Key R & D programs of the Ministry of Science and Technology of China (No.2021YFE0115800) and the National Science Funding Committee of China (No. U20A20250). the programs of the science and technology of Yulin City (No. CXY-2023-ZX04), and the funding support from Shccig-Qinling Program.

Notes: The authors declare no competing financial interest.

References

1. Qiu, Y.; Rao, Y. F.; Zheng, Y. N.; Hu, H.; Zhang, W. H.; Guo, X. H., Activating ruthenium dioxide via compressive strain achieving efficient multifunctional electrocatalysis for Zn-air batteries and overall water splitting. Infomat 2022, 4 (9), e12326.
2. Yao, H.; Zheng, Y. A.; Yue, S. L.; Hu, S. J.; Yuan, W. Y.; Guo, X. H., B-site substitution in $NaCo_{1-2x}Fe_xNi_xF_3$ perovskites for efficient oxygen evolution. Inorg Chem Front 2023, 10 (3), 804-814.

 doi:10.20944/preprints202409.2438.v1

3. Diao, J. X.; Qiu, Y.; Liu, S. Q.; Wang, W. T.; Chen, K.; Li, H. L.; Yuan, W. Y.; Qu, Y. T.; Guo, X. H., Interfacial Engineering of WN/WC Heterostructures Derived from Solid-State Synthesis: A Highly Efficient Trifunctional Electrocatalyst for ORR, OER, and HER. Adv Mater 2020, 32 (7), 1905679.
4. Yu, M. Q.; Budiyanto, E.; Tüysüz, H., Principles of Water Electrolysis and Recent Progress in Cobalt-, Nickel-, and Iron-Based Oxides for the Oxygen Evolution Reaction. Angew Chem Int Ed 2022, 61 (1), e202103824.
5. Zhang, K. X.; Zou, R. Q., Advanced Transition Metal-Based OER Electrocatalysts: Current Status, Opportunities, and Challenges. Small 2021, 17 (37), 2100129.
6. Nam, D.; Kim, J., Development of NiO/CoO nanohybrids catalyst with oxygen vacancy for oxygen evolution reaction enhancement in alkaline solution. Int J Hydrogen Energy 2022, 47 (38), 16900-16907.
7. Zhou, D. J.; Li, P. S.; Lin, X.; McKinley, A.; Kuang, Y.; Liu, W.; Lin, W. F.; Sun, X. M.; Duan, X., Layered double hydroxide-based electrocatalysts for the oxygen evolution reaction: identification and tailoring of active sites, and superaerophobic nanoarray electrode assembly. Chem Soc Rev 2021, 50 (15), 8790-8817.
8. Zou, X.; Liu, Y.; Li, G.-D.; Wu, Y.; Liu, D.-P.; Li, W.; Li, H.-W.; Wang, D.; Zhang, Y.; Zou, X., Ultrafast Formation of Amorphous Bimetallic Hydroxide Films on 3D Conductive Sulfide Nanoarrays for Large-Current-Density Oxygen Evolution Electrocatalysis. Adv Mater 2017, 29 (22), 1700404.
9. Luo, R.; Qian, Z.; Xing, L.; Du, C.; Yin, G.; Zhao, S.; Du, L., Re-Looking into the Active Moieties of Metal X-ides (X- = Phosph-, Sulf-, Nitr-, and Carb-) Toward Oxygen Evolution Reaction. Adv. Funct. Mater. 2021, 31 (37), 2102918.
10. Lei, H.; Cui, M. W.; Huang, Y., S-Doping Promotes Pyridine Nitrogen Conversion and Lattice Defects of Carbon Nitride to Enhance the Performance of Zn-Air Batteries. Acs Appl Mater Inter 2022, 14 (30), 34793-34801.
11. Lee, Y. J.; Park, S.-K., Metal–Organic Framework-Derived Hollow CoS Nanoarray Coupled with NiFe Layered Double Hydroxides as Efficient Bifunctional Electrocatalyst for Overall Water Splitting. Small 2022, 18 (16), 2200586.
12. Wang, T.; Wang, W. W.; Shao, W. J.; Bai, M. R.; Zhou, M.; Li, S.; Ma, T.; Ma, L.; Cheng, C.; Liu, X. K., Synthesis and Electronic Modulation of Nanostructured Layered Double Hydroxides for Efficient Electrochemical Oxygen Evolution. Chemsuschem 2021, 14 (23), 5112-5134.
13. Gong, M.; Li, Y. G.; Wang, H. L.; Liang, Y. Y.; Wu, J. Z.; Zhou, J. G.; Wang, J.; Regier, T.; Wei, F.; Dai, H. J., An Advanced Ni-Fe Layered Double Hydroxide Electrocatalyst for Water Oxidation. J Am Chem Soc 2013, 135 (23), 8452-8455.
14. Hu, Y. D.; Luo, G.; Wang, L. G.; Liu, X. K.; Qu, Y. T.; Zhou, Y. S.; Zhou, F. Y.; Li, Z. J.; Li, Y. F.; Yao, T.; Xiong, C.; Yang, B.; Yu, Z. Q.; Wu, Y., Single Ru Atoms Stabilized by Hybrid Amorphous/Crystalline FeCoNi Layered Double Hydroxide for Ultraefficient Oxygen Evolution. Adv. Energy Mater. 2021, 11 (1), 2002816.
15. Li, Z. S.; Xiao, K. C.; Yu, C. L.; Wang, H. Q.; Li, Q. Y., Three-dimensional graphene-like carbon nanosheets coupled with MnCo-layered double hydroxides nanoflowers as efficient bifunctional oxygen electrocatalyst. Int J Hydrogen Energy 2021, 46 (69), 34239-34251.
16. Wang, X.; He, Y. Y.; Zhou, Y. S.; Li, R. K.; Lu, W. P.; Wang, K. K.; Liu, W. K., In situ growth of NiCoFe-layered double hydroxide through etching Ni foam matrix for highly enhanced oxygen evolution reaction. Int J Hydrogen Energy 2022, 47 (56), 23644-23652.
17. Wang, K. X.; Wang, X. Y.; Li, Z. J.; Yang, B.; Ling, M.; Gao, X.; Lu, J. G.; Shi, Q. R.; Lei, L. C.; Wu, G.; Hou, Y., Designing 3d dual transition metal electrocatalysts for oxygen evolution reaction in alkaline electrolyte: Beyond oxides. Nano Energy 2020, 77, 105162.
18. Yang, Y.; Xie, Y. C.; Yu, Z. H.; Guo, S. S.; Yuan, M. W.; Yao, H. Q.; Liang, Z. P.; Lu, Y. R.; Chan, T. S.; Li, C.; Dong, H. L.; Ma, S. L., Self-supported NiFe-LDH@CoS nanosheet arrays grown on nickel foam as efficient bifunctional electrocatalysts for overall water splitting. Chem. Eng. J. 2021, 419, 129512.
19. Lai, F. L.; Miao, Y. E.; Zuo, L. Z.; Lu, H. Y.; Huang, Y. P.; Liu, T. X., Biomass-Derived Nitrogen-Doped Carbon Nanofiber Network: A Facile Template for Decoration of Ultrathin Nickel-Cobalt Layered Double Hydroxide Nanosheets as High-Performance Asymmetric Supercapacitor Electrode. Small 2016, 12 (24), 3235-3244.

 doi:10.20944/preprints202409.2438.v1

20. Jia, Y.; Zhang, L. Z.; Gao, G. P.; Chen, H.; Wang, B.; Zhou, J. Z.; Soo, M. T.; Hong, M.; Yan, X. C.; Qian, G. R.; Zou, J.; Du, A. J.; Yao, X. D., A Heterostructure Coupling of Exfoliated Ni-Fe Hydroxide Nanosheet and Defective Graphene as a Bifunctional Electrocatalyst for Overall Water Splitting. Adv Mater 2017, 29 (17), 1700017.
21. Meng, W.; He, H. Y.; Yang, L.; Jiang, Q. G.; Yuliarto, B.; Yamauchi, Y.; Xu, X. T.; Huang, H. J., 1D-2D hybridization: Nanoarchitectonics for grain boundary-rich platinum nanowires coupled with MXene nanosheets as efficient methanol oxidation electrocatalysts. Chem. Eng. J. 2022, 450, 137932.
22. Yang, C. Z.; Huang, H. J.; He, H. Y.; Yang, L.; Jiang, Q. G.; Li, W. H., Recent advances in MXene-based nanoarchitectures as electrode materials for future energy generation and conversion applications. Coord Chem Rev 2021, 435, 213806.
23. Wang, W.; Liu, Y. C.; Li, J.; Luo, J.; Fu, L.; Chen, S. L., NiFe LDH nanodots anchored on 3D macro/mesoporous carbon as a high-performance ORR/OER bifunctional electrocatalyst. J. Mater. Chem. A 2018, 6 (29), 14299-14306.
24. Rinawati, M.; Wang, Y. X.; Huang, W. H.; Wu, Y. T.; Cheng, Y. S.; Kurniawan, D.; Haw, S. C.; Chiang, W. H.; Su, W. N.; Yeh, M. H., Unraveling the efficiency of heteroatom-doped graphene quantum dots incorporated MOF-derived bimetallic layered double hydroxide towards oxygen evolution reaction. Carbon 2022, 200, 437-447.
25. Zhi, D. D.; Li, T.; Li, J. Z.; Ren, H. S.; Meng, F. B., A review of three-dimensional graphene-based aerogels: Synthesis, structure and application for microwave absorption. Composites, Part B 2021, 211, 108642.
26. Dang, A. L.; Liu, X.; Wang, Y. J.; Liu, Y. H.; Cheng, T.; Zada, A.; Ye, F.; Deng, W. B.; Sun, Y. T.; Zhao, T. K.; Li, T. H., High-efficient adsorption for versatile adsorbates by elastic reduced graphene oxide/Fe3O4 magnetic aerogels mediated by carbon nanotubes. J. Hazard. Mater. 2023, 457, 131846.
27. Huang, Y. L.; Wei, Q. L.; Wang, Y. Y.; Dai, L. Y., Three-dimensional amine-terminated ionic liquid functionalized graphene/Pd composite aerogel as highly efficient and recyclable catalyst for the Suzuki cross-coupling reactions. Carbon 2018, 136, 150-159.
28. Zheng, Z. C.; Wu, D.; Chen, G.; Zhang, N.; Wan, H.; Liu, X. H.; Ma, R. Z., Microcrystallization and lattice contraction of NiFe LDHs for enhancing water electrocatalytic oxidation. Carbon Energy 2022, 4 (5), 901-913.
29. Chen, W. Y.; Han, B.; Xie, Y. L.; Liang, S. J.; Deng, H.; Lin, Z., Ultrathin Co-Co LDHs nanosheets assembled vertically on MXene: 3D nanoarrays for boosted visible-light-driven CO reduction. Chem. Eng. J. 2020, 391, 123519.
30. Kim, J. H.; Ko, Y. I.; Lee, S. Y.; Lee, Y. S.; Kim, S. K.; Kim, Y. A.; Yang, C. M., Ni-Co layered double hydroxide coated on microsphere nanocomposite of graphene oxide and single-walled carbon nanohorns as supercapacitor electrode material. Int J Energy Res 2022, 46 (15), 23564-23577.
31. Linghu, W. S.; Yang, H.; Sun, Y. X.; Sheng, G. D.; Huang, Y. Y., One-Pot Synthesis of LDH/GO Composites as Highly Effective Adsorbents for Decontamination of U(VI). Acs Sustain Chem Eng 2017, 5 (6), 5608-5616.
32. Wu, Y. J.; Song, M. L.; Huang, Y. C.; Dong, C. L.; Li, Y. Y.; Lu, Y. X.; Zhou, B.; Wang, D. D.; Jia, J. F.; Wang, S. Y.; Wang, Y. Y., Promoting surface reconstruction of NiFe layered double hydroxides via intercalating $[Cr(C_2O_4)_3]_3$-for enhanced oxygen evolution. J Energy Chem 2022, 74, 140-148.
33. Si, S.; Hu, H. S.; Liu, R. J.; Xu, Z. X.; Wang, C. B.; Feng, Y. Y., Co-NiFe layered double hydroxide nanosheets as an efficient electrocatalyst for the electrochemical evolution of oxygen. Int J Hydrogen Energy 2020, 45 (16), 9368-9379.
34. Yan, L.; Du, Z. P.; Lai, X. Y.; Lan, J. Y.; Liu, X. J.; Liao, J. Y.; Feng, Y. F.; Li, H., Synergistically modulating the electronic structure of Cr-doped FeNi LDH nanoarrays by O-vacancy and coupling of MXene for enhanced oxygen evolution reaction. Int J Hydrogen Energy 2023, 48 (5), 1892-1903.
35. Yin, P. Q.; Wu, G.; Wang, X. Q.; Liu, S. J.; Zhou, F. Y.; Dai, L.; Wang, X.; Yang, B.; Yu, H. Q., NiCo-LDH nanosheets strongly coupled with GO-CNTs as a hybrid electrocatalyst for oxygen evolution reaction. Nano Research 2021, 14 (12), 4783-4788.
36. Shen, B. F.; Feng, Y.; Wang, Y.; Sun, P. Y.; Yang, L.; Jiang, Q. G.; He, H. Y.; Huang, H. J., Holey MXene nanosheets intimately coupled with ultrathin Ni-Fe layered double hydroxides for boosted hydrogen and oxygen evolution reactions. Carbon 2023, 212, 118141.
37. Wan, C. W.; Jin, J.; Wei, X. Y.; Chen, S. Z.; Zhang, Y.; Zhu, T. L.; Qu, H. X., Inducing the SnO based electron transport layer into NiFe LDH/NF as efficient catalyst for OER and methanol oxidation reaction. J. Mater. Sci. Technol. 2022, 124, 102-108.

 doi:10.20944/preprints202409.2438.v1

38. Fan, K.; Chen, H.; Ji, Y. F.; Huang, H.; Claesson, P. M.; Daniel, Q.; Philippe, B.; Rensmo, H.; Li, F. S.; Luo, Y.; Sun, L. C., Nickel-vanadium monolayer double hydroxide for efficient electrochemical water oxidation. Nat Commun 2016, 7,11981.
39. Zhou, Y. N.; Yu, W. L.; Cao, Y. N.; Zhao, J.; Dong, B.; Ma, Y.; Wang, F. L.; Fan, R. Y.; Zhou, Y. L.; Chai, Y. M., S-doped nickel-iron hydroxides synthesized by room-temperature electrochemical activation for efficient oxygen evolution. Appl. Catal., B 2021, 292, 120150.
40. He, J.; Zhou, X.; Xu, P.; Sun, J. M., Promoting electrocatalytic water oxidation through tungsten-modulated oxygen vacancies on hierarchical FeNi-layered double hydroxide. Nano Energy 2021, 80, 105540.
41. Wang, Y.; Zhao, Y. Z.; Liu, L.; Qin, W. J.; Liu, S. J.; Tu, J. P.; Qin, Y. P.; Liu, J. F.; Wu, H. Y.; Zhang, D. Y.; Chu, A. M.; Jia, B. R.; Qu, X. H.; Qin, M. L., Mesoporous Single Crystals with Fe-Rich Skin for Ultralow Overpotential in Oxygen Evolution Catalysis. Adv Mater 2022, 34 (20), 2200088.